Astron. Astrophys. 319, 267–273 (1997)

ASTRONOMY
AND
ASTROPHYSICS

M 2-9: moving dust in a fast bipolar outflow⋆

Hugo E. Schwarz[1,2], **Colin Aspin**[1,3], **Romano L.M. Corradi**[4], **and Bo Reipurth**[2]

[1] Nordic Optical Telescope, Apartado 474, Sta. Cruz de La Palma, Canarias, Spain
[2] ESO, Casilla 19001, Santiago 19, Chile
[3] Joint Astronomy Centre, 660 A'ohoku Pl., Hilo, Hawaii 96720, USA
[4] IAC, Via Lactea, E-38200 La Laguna, Tenerife, Canarias, Spain

Received 29 April 1996 / Accepted 30 July 1996

Abstract. Using optical images and spectra of the bipolar nebula M 2-9 we show that, in addition to the well-known bright inner nebula, the object has fast, highly collimated outflows reaching a total extent of 115 ″. These radially opposed and point-symmetric outer lobes are *both* redshifted, leading us to model the radiation from them in terms of light reflected from moving dust, rather than intrinsic emission. Our polarization images show that the lobes are 60% linearly polarized in a direction perpendicular to the long axis of M 2-9. This high polarization indicates optically thin scattering, and lends weight to our dust scattering model.

Use of this model then allows us to determine the distance to M 2-9 directly from the measured proper motions on images taken over a period of more than 16 yrs. The physical and geometrical parameters of the nebula then follow. M 2-9 is at a distance of 650 pc, is 0.4 pc long, has a luminosity of 550 $L_\odot$, and its outer nebula has a dynamical age of 1200 yrs, in round numbers.

Using the fact that the central object has been constrained to be of low luminosity but of a sufficiently high temperature to make the observed OIII, we argue that the central object of M 2-9 has to contain a compact, hot source, and is probably a binary.

Key words: ISM: M 2-9 – planetary nebulae: M 2-9 – ISM: jets and outflows – polarisation – dust – circumstellar matter

1. Introduction

M 2-9 is a well studied galactic nebula featuring in nearly 200 entries in the SIMBAD database. M 2-9 was discovered by Minkowski (1947) and has since then been described as a planetary nebula (PN) in formation (Allen & Swings 1972), a BQ radio star (Ciatti & Mammano 1975), an eruptive star (Balick 1989); it has been related to symbiotics (Lutz et al. 1989), and to Be stars (Swings & Andrillat 1979). At present the consensus is that M 2-9 is an evolved object, probably a PN in formation or a proto-PN (PPN).

The properties of the 40″ long "butterfly" nebula have been studied in detail in a series of papers by Allen & Swings (1972), van den Bergh (1974), Walsh (1981), Carsenti & Solf (1983), Aspin & McLean (1984), Goodrich (1991), and Trammell et al. (1995). In 1980, Kohoutek & Surdej (hereafter KS80) discovered two very faint emission loops associated with M 2-9 on an ESO 3.6m telescope prime focus photographic plate taken in 1978, after which no further work on these outer parts of the nebula has been published. It is just these faint, highly collimated loops that we will concentrate on in this paper.

2. Results and observations: the faint lobes reveal

2.1. Imaging and spectroscopy: high collimation and velocity

Fig. 1 shows a narrow band Hα image of M 2-9 taken with EMMI on the ESO NTT telescope at La Silla on 91.07.04. The image shown is a median filtered average of three 600^s exposures taken through a filter with central wavelength 656.8 nm and a FWHM of 7.33 nm. The image therefore includes in addition to the Hα line some of the light from the [NII]658.4nm line. The image diameters of stars measured on this image are 0.″8 FWHM. Note the detailed structure in the inner nebula, which is displayed with different cut levels from those of the rest of the image, to bring out the faint loops more clearly.

The first feature one can see in the image is the high degree of collimation of the loops. They have an aspect ratio of 10.3 indicating that a strongly collimating mechanism is operating in M 2-9.

The loops are limb brightened, probably because they are hollow shells of swept up matter. The northern loop end or ansa is fainter than the southern one by a factor of 2. This ratio has been determined using photometry in a circular software aperture with a diameter of 8″centred on the bright loop ends.

Send offprint requests to: H. E. Schwarz, at the NOT address

⋆ Based on observations made at the European Southern Observatory.

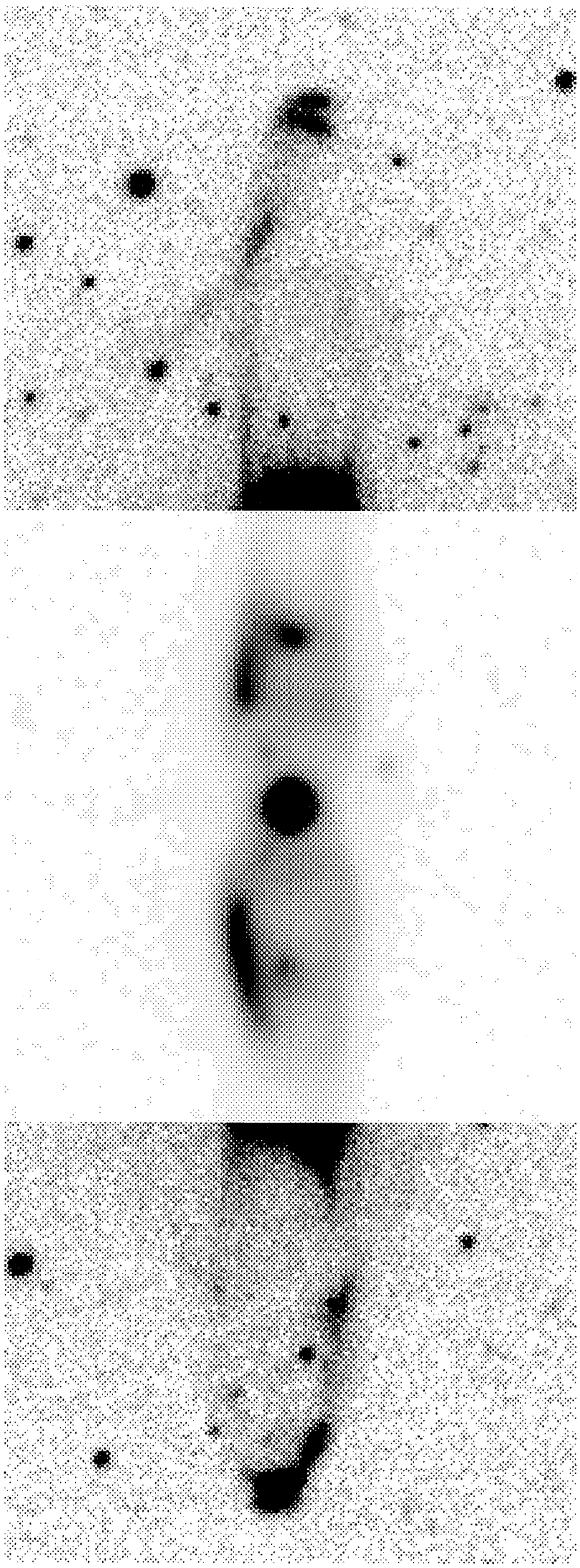

Fig. 1. Narrowband Hα image of M 2-9 showing the detailed structure of both the inner nebula and the faint outer loops. Two different cut levels have been used to overcome the large dynamic range of the object. The image is 49″ by 131″ and stars in the image have diameters of 0.8″ FWHM. North is up, east is to the left.

The brightness distribution within the outer part of both loops is not symmetrical about the long axis of M 2-9: the southern loop is brighter on its western side, the northern one on the east. For this reason, the loops do not define a plane of symmetry passing through the central object as would be expected in a purely bipolar object. Lines passing through equivalent parts of both loops also pass through the central object: we have *point-symmetry* instead of *plane-symmetry*. This places M 2-9 in a special class of objects defined by Schwarz et al.(1993). A natural explanation for the formation mechanism of such objects was discussed in Schwarz (1994), and is discussed in more detail in Sect. 2.7 of this paper.

The point-symmetry is more clearly shown in the contour plot of Fig. 2. Other features in the loops are: both end caps or ansae are double, in the shape of a "hamburger"; the northern loop shows part of a circular arc at about 40″ from the central object. Its counterpart in the southern loop is only marginally detected.

Fig. 3 shows the long slit spectrum of M 2-9 taken on 91.07.04 with EMMI attached to the NTT. The grating used (EMMI No.6) gives a reciprocal dispersion of 0.042nm pixel^{-1} on the 15μm square pixels of the Ford 2048^2 CCD. With our slit width of 1″ projecting onto 3 pixels, the effective resolution of the spectrum is 0.12nm. Stronger emission lines can be centroided to about 0.1 pixel, giving a velocity resolution of about 2 km.s^{-1}. The spectrum shown here is a median filtered average of three 30 minute exposures taken with the slit aligned with the long axis of M 2-9, which is approximately at PA 180^o, so that *south is up in Fig. 3*.

The total wavelength ranges from 654nm to 673nm, of which about 7.5nm are shown in Fig. 3. From this spectrum, the radial velocities of the outer loops have been determined. *Both loops are redshifted*, as had previously been noted by Schwarz (1990) and Solf (1993). For axial outflows from an object with its axis inclined to the plane of the sky at some non-zero angle, one expects a red and a blue shifted side. This assumes that the radiation comes from the outflowing gas and shares its red or blue shift with that of the gas. The observed redshifts amount to 275 km.s^{-1} and 188 km.s^{-1} for respectively the north and south loop ends. These velocities include the radial velocity of the whole system of central object and nebulae, which we measured to be 79 km.s^{-1}. All radial velocities reported here are heliocentric.

An object with the two loops emerging at an angle significantly different from 180^o, and which happen to be oriented away from us, and at near 90^o to the plane of the sky could explain the observed redshifts. This is physically as well as statistically extremely unlikely. Another way of explaining the redshifts is by having an object with one loop being outflow the other being inflow (!), which is even more unlikely.

Our preferred explanation is that the loop ends (ansae) contain dust which scatters the light coming from the central object. This model makes some predictions: a) the scattered light should show the projected outflow velocity as a redshift in both "ansae" since both act as mirrors which are travelling away from the central object. b) assuming that the ansae have the same space

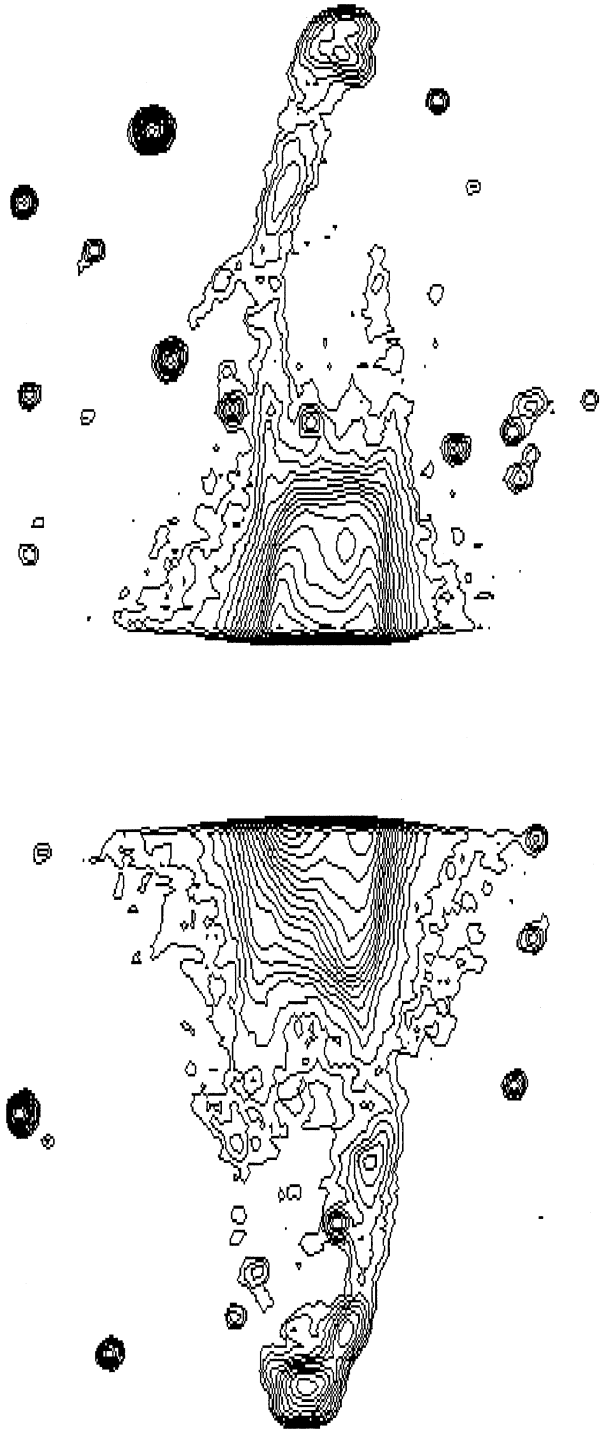

Fig. 2. The contour plot of the outer lobes of M 2-9 at the same scale as in Fig. 1 but excluding the bright inner part. The point-symmetry of the loops is clearly seen. The contour levels start at 7 ADUs above the mean sky background value (= 8 ADUs), and increase in 17 steps of a factor of $2^{0.5}$ up to 2892 ADUs. North is up and east is to the left.

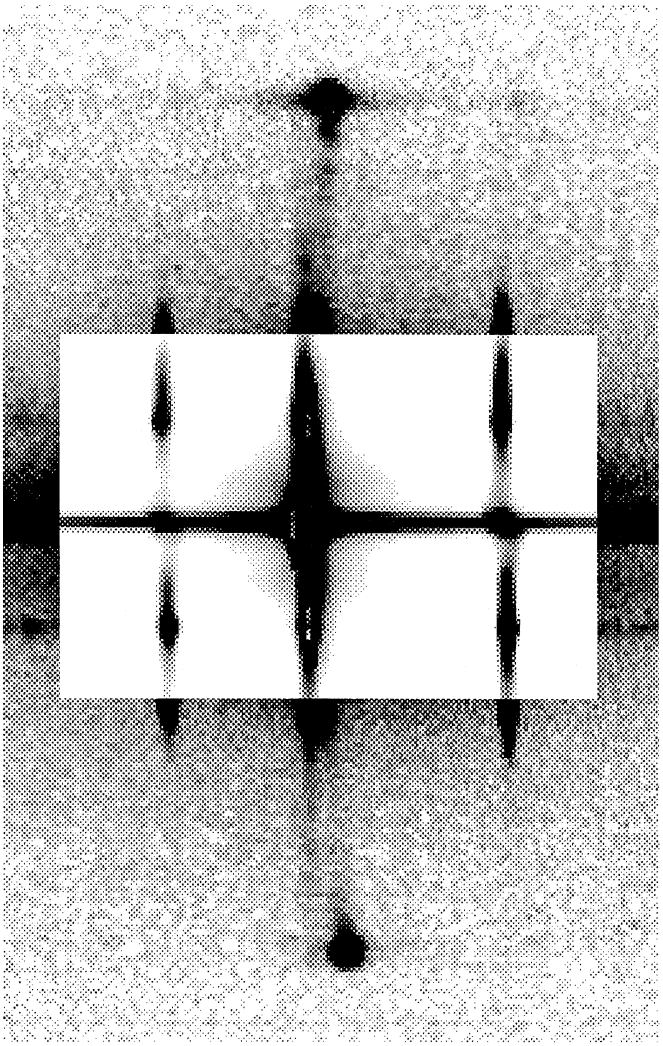

Fig. 3. The long-slit spectrum of M 2-9. The PA of the slit was 180^o, so that the spatial axis runs vertically spanning $136''$with south towards the top, and wavelength increases from left to right, covering 6.9nm centred on the Hα, [NII]654.8 and 658.3 lines. Note that the strongest [NII] line is also detected in the southern outer loop. The central part of the Hα line is saturated.

velocity, one should have a higher redshift than the other because of the projection effects of the inclination of the object. In one case the projected velocity adds, in the other case it vectorially subtracts from the redshift of the lobes themselves. c) the light from the ansae should have a spectrum similar to that of the central illuminating object. d) and most importantly, the light from the ansae should be highly polarized at right angles to the long axis of the object if the angle to the line of sight (i.e. the scattering angle) is sufficiently close to 90^o. The last point seems plausible from the aspect of the object; it is viewed near the plane of the sky or the lobes would show projection overlap, which is not the case here.

The point (a) about the redshifts has been observed, and the northern ansa has a higher radial velocity than the southern one (b). The spectra of the ansae are dominated by Hα line emis-

sion flanked by a very faint pair of [NII] lines. This is due to the fact that the strongest line by a factor of more than 10 in our spectrum of the central object is Hα, and the much fainter reflected light would therefore only show this line (c). By taking a very deep spectrum we have also observed other, weaker lines and extended wings in the Hα line. Since these wings have also been observed in the central object (Balick 1989) their presence in the outer lobes strengthens the case for reflection. Their ratio to the lines in the central object will depend on the exact wavelength dependence of the scattering mechanism operating in the lobes. This will allow a more profound study of the properties of the ansae as a function of wavelength. There is no indication, therefore, that the ansae are producing other spectral features which are not in the reflected light. Point (d), the observed high degree of polarization of the light is discussed in detail below.

2.2. Polarimetry: reflecting dust

Using the polarimetric mode of EFOSC1, the images shown in Fig. 4 have been obtained. By processing the orthogonally polarized strips with the appropriate algorithms (e.g. Schwarz 1984), the percentage and position angle of polarization have been determined. The northern lobe is 62% polarized at an (approximately equatorial) angle of 91.3^o, while the southern lobe shows 59% at 94.6^o. The errors are about $\pm$ 2.5% on the percentage and 1.2^o on the angle of polarization. Measurements of serendipitous field stars indicate that the instrumental polarization is less than 2%, and can therefore be neglected in comparison to the 60% results reported above.

Clearly, the very high degree of polarization proves that there is dust present, that it must be optically thin and that the average scattering angle is near 90^o with a relatively small spread around its value. If the dust were optically thick, the linear polarization would be reduced by multiple scattering and linear to circular conversion would take place. 60% is such a high value that the material must be optically thin. The fact that the polarization angle is nearly perpendicular to the long axis of the object is also a strong indicator of scattering: in both Rayleigh and Mie scattering the polarization vector is expected to be perpendicular to the scattering plane, formed in this case by the central object, the ansa in question, and the observer.

Note that Code & Whitney(1995) have made calculations that showed the maximum polarization degree from dust scattering to be 50%. This indicates that at least some Rayleigh scattering has to be present.

All four predictions of our dust model have indeed been observed and we therefore proceed to use the model to derive the fundamental parameters of M 2-9.

2.3. The reflective dust model: inclination and space velocity

Fig. 5 shows a sketch of the reflective dust model of M 2-9.

If we assume that some dust from the inner parts of M 2-9 has been swept up by a fast outflow, or that the dust was present further out due to the presence of a fossile PN and was taken along from there, the end result is that the outer part of the loops now contains dust. After subtracting the heliocentric system radial velocity of 79km.s^{-1} from all measured radial velocities, the following hold:

$$V_N = V_{exp} + V_{exp} \sin i$$

$$V_S = V_{exp} - V_{exp} \sin i$$

where V_N and V_S are respectively the northern and southern observed radial velocities, V_{exp} is the velocity of recession of the ansae with respect to the central object, and *i* is the angle between the object's long axis and the plane of the sky.

The vectorial addition of these velocities is allowed because of the reflection of the light from the central object from the dust in each ansa. Putting in the observed V_N and V_S, gives the inclination of M 2-9 as 15^o where the northern loop points away from the observer. Compare this value with the 11^o derived by Goodrich (1991) for the inner nebula. Applying the same analysis to our data on the inner nebula, we obtain an inclination angle of 31^o. This difference can be explained by assuming that the reflected light that forms the inner nebula comes off the front and back of the hollow lobes. The width to length ratio of these inner emissions is such that the possible angle of the projected velocity is 18^o either way. Subtracting this from the observed 31^o gives 13^o, which agrees with Goodrich's result to within the uncertainties. Note that if the inner nebula is indeed due to some "lighthouse effect" reflecting off the lobes, it will be interesting

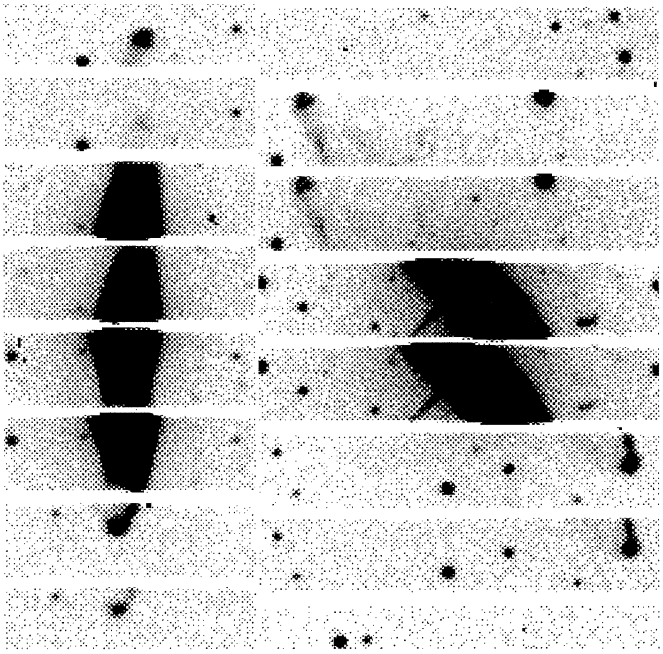

Fig. 4. The polarimetric Hα images of M 2-9. On the left the alternate strips show the polarized flux parallel and perpendicular to the long axis of the nebula; on the right the strips are at $\pm$ 45^o to this axis. Note that due to the polarization vector being perpendicular to the nebular axis, the orthogonally polarized images on the left show strong intensity differences, while those on the right do not. The level of polarization is 60%, hence the strong effect on the images.

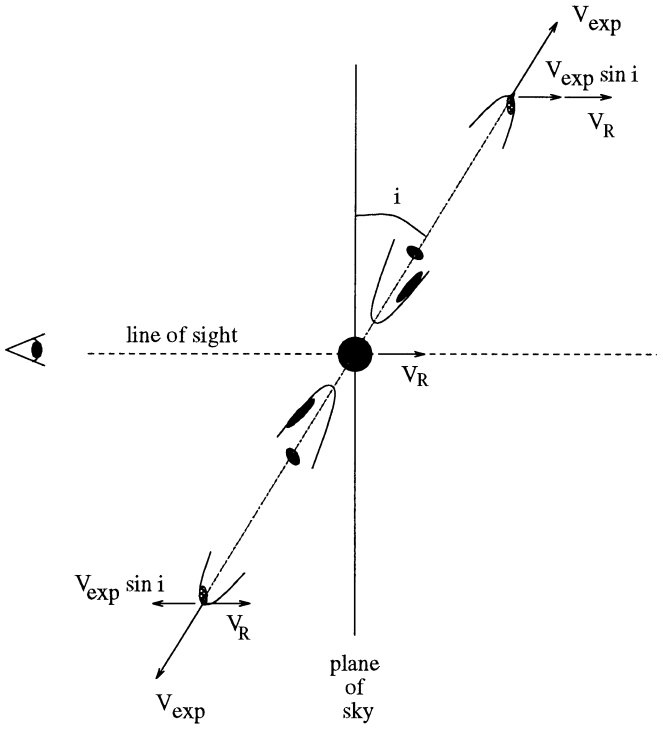

Fig. 5. The reflective dust model for M 2-9. Indicated are the observer, the line of sight, the plane of the sky, and schematically the faint loops. North is at the top. The velocity vectors are not drawn to scale.

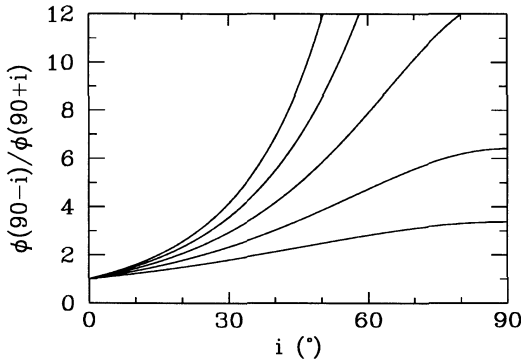

Fig. 6. Plot of the phase function intensity ratio ϕ(90-i)/ϕ(90+i) against i, the inclination angle on the sky of M 2-9. The intersection of the observed ratio of 2 with the ratio curve gives the angle i. Curves for several different values of the asymmetry factor in the phase function are plotted; lower-most curve corresponds to 0.2, increasing in steps of 0.1 to 0.6 (uppermost curve). This compares well with the 15^o we found from the geometrical analysis above.

to repeat this measurement after about half a rotation period of these features. This period is 70-75 yrs from the differences seen in images taken in 1952, 1971, and 1978 (see Allen & Swings 1972, van den Bergh 1974 and KS80), but its coherence time is unknown. A different inclination angle from the present one should then be found.

The expansion velocity of the outer ansae is 164 km.s^{-1}, which is the true space velocity of expansion of the ansae. The inner nebula has an expansion velocity of 23km.s^{-1}.

2.4. Scattering function: an independent check on the inclination

The scattering phase function can provide us with an independent determination of the inclination angle on the sky, i, that was derived in a purely geometrical way in Sect. 2.2 above. By considering the usual phase function for scattering off interstellar dust (Henyey & Greenstein 1941), ϕ, say, the scattered intensity from the two lobes must be different because the scattering angles are different. The northern lobe has ϕ(90+i), the southern one has ϕ(90-i), and we have measured the intensity from the two lobes to have a ratio of 2, whereby the southern lobe is the brighter of the two. By plotting ϕ(90-i)/ϕ(90+i) against i for various reasonable asymmetry factors in the phase function, we can read off the inclination angle for which the ratio is equal to 2. This plot is shown in Fig. 6, and the value for i found is in the range 13^o to 22^o for a range of asymmetry factors of 0.2 to 0.6. Note that the generally assumed value for interstellar dust at the Hα wavelength is $\sim$0.4 (Di Bartolomeo et al. 1996), giving an angle of 19^o. This agrees within the uncertainties with the geometrical value of 15^o.

2.5. Proper motion: the distance

Using the earliest (discovery) image of the faint lobes, and our own recent data, we have determined the proper motion of the brightest outer parts of the lobes. Here we use 5 images: a 3.6m telescope prime focus photograph taken on 78.04.15 and published by KS80, a CCD image taken on 86.03.18 with the Danish 1.54m telescope, a CCD image taken with the adapter at the 2.2m telescope on 88.07.17, a CCD image taken on 91.07.04 with EMMI on the NTT, and our most recent image from the 3.6m with EFOSC1 taken on 94.06.10. The data span a period of 16.15 yrs, and from accurate determinations of the positions of the Gaussian peak of the brighter features at the ends of the faint lobes, we have found a total expansion of $0\farcs82 \pm 0\farcs1$, or $0\farcs051$ .yr^{-1} $\pm$ $0\farcs007$ .yr^{-1}. Fig. 5 shows a plot of the expansion versus time.

By deprojecting the measured expansion velocity, $2V_{exp}$ = 328 km.s^{-1}, we obtain for the velocity in the plane of the sky a value of 317 km.s^{-1}. This velocity combined with the measured proper motion, and assuming the above dust reflection model, gives us the distance directly: M 2-9 is at 640pc. The range for the distance is 563pc $\leq$ d $\leq$ 743pc mainly due to the errors on the angular position measurements, but including a small component due to the errors on the velocity measurement. Note that the previously published distances have range of a factor of 106 (!): from the 50pc of KS80 to the 5.3kpc of Barker (1978), with a mean of about 3kpc or so, giving ranges in luminosity and nebular mass of respectively 11200 and 1.2 million. Clearly, as for nearly all PNe, the accurate distance of M 2-9 is a crucial datum!

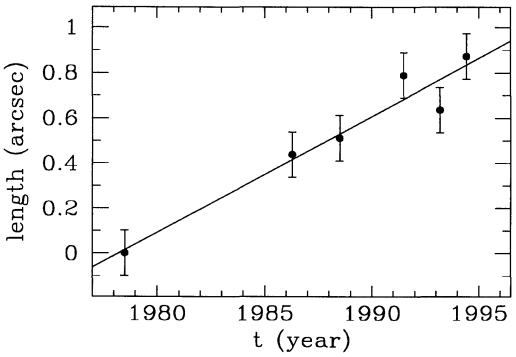

Fig. 7. Plot of the projected length normalised to Kohoutek's 1978 image on the sky of M 2-9 versus time. The errorbars are estimates of the accuracy of determining the position of the peak of a 2-dimensional Gaussian fit.

Table 1. Summary of properties of M 2-9.

Parameter	lower limit	value	upper limit
distance (pc)	563	**640**	742
size (pc)	0.32	**0.37**	0.43
luminosity ($L_\odot$)	428	**553**	743
dyn. age (yrs)	1013	**1171**	1361

2.6. Luminosity, nebular size, dynamical age

Now we have the distance, we can calculate some other parameters of the object. By integrating the flux distribution from the optical out to 100μm, and adding our 1.3mm data point and some radio data at longer wavelengths from Acker et al. (1992), we determine a (more or less) bolometric luminosity for M 2-9 of L= $1.35.10^{-3}$d^2(pc) $L_\odot$. At 640pc this becomes L = 553 $L_\odot$. The range of luminosity based on the errors discussed above then is: 428 $L_\odot \leq$ L $\leq$ 743 $L_\odot$. For the size of the nebula's long axis we obtain 0.37pc with a range of 0.32pc $\leq$ l $\leq$ 0.43pc again mainly set by the errors on the proper motion. The dynamical age of the outer nebula, under the assumption that the expansion velocity has been constant during its lifetime, is t = 1171 yrs with a range 1013 yrs $\leq$ t $\leq$ 1361 yrs. Summarising these results, we list them in Table 1.

The luminosity found is low for a typical AGB star. A main-sequence B star with a temperature of 35000K has been suggested for the central object of M 2-9. If this were so, M 2-9 would be placed at a distance of about 2.3kpc. This is clearly far outside the determined range for the distance and effectively rules out such a star for M 2-9. If there is a main-sequence star in M 2-9 its bolometric luminosity should lie in the above found range. This corresponds to a narrow range around a B5 star. With a temperature of about 15000K such a star could not doubly ionise oxygen to produce the observed [OIII] line emission in the spectrum (e.g Calvet & Cohen 1978). Thus a B5 star cannot be the only energy source in M 2-9. Other, more exotic possibilities are discussed below.

2.7. Speculation: central object, density, mass, and dust properties

The impossibility of having a single B5 main sequence star as energy source for M 2-9 because of its low temperature, makes us suggest that a compact but hot component must be present. This possible binary central object explains all that has been observed: the hot component ionises the high excitation emission lines; the B5 (or cooler) star provides part of the luminosity; and the binary interaction of the pair has produced the high collimation of the nebula. An accretion disk around the compact star provides the fast disk wind that sweeps up previously lost dust which we see in the form of the faint outer lobes because of light scattered from the beam from the central object.

Some idea about the density of the nebula can be obtained by assuming that the limb brightened edges (not the ansae) of the loops are luminous because of photo ionisation. Then the surface brightness is roughly proportional to the column density. By comparing the surface brightness of the inner with that of the outer nebula we can get a rough ratio of the inner and outer nebular densities. Inner nebular densities are on the order of 10^5cm^{-3} (Calvet & Cohen 1978) giving a range for the edge density in the outer loops of between 2 and 10.10^2 cm^{-3}. Taking a thickness of the outer shell estimated from our images of about 3 pixels or $1.7.10^{14}$m, and approximating the nebula as a cylinder of length 0.37pc, and diameter 0.036pc, we get a total mass for the outer lobes in the range 0.0011 to 0.0056 $M_\odot$. Since a star loses a significant fraction of a solar mass during its ascent of the AGB, these values of less than one percent of a solar mass for the swept up material are plausible albeit highly uncertain.

Some of the properties of the dust at the ends of the loops can be determined as follows. By measuring the ratio of the Hα flux from the ansae and that from the central object we can calculate the geometrical scattering efficiency of the dust, assuming that the unscattered radiation simply escapes from the object. Heating or conversion into IR emission is not considered here. IR imaging observations made by us indicate that the IR emission from the ansae is very weak in comparison with the optical emission, and reprocessing of radiation can therefore not play a major role.

Some evidence that the extinction intrinsic to M 2-9 along its equatorial plane is much higher than that in the polar directions is provided by the following observation. Considering a sphere centred on M 2-9 with a radius equal to the extent of the faint loops, the relative area covered by an ansa is about $3.5.10^{-4}$. The ratio between the mean flux from the ansae and that from the central object is about 0.001. This implies that the ratio between the equatorial and the polar extinction is at least a factor of 3, and probably much higher.

2.8. Jets from evolved and from young stars

The bipolar pair of jets in M 2-9 represents one of the most collimated outflows known so far from an evolved star. If we adopt a size for the ansae of about a third the width of the loops

themselves (see Fig. 1), their effective aspect ratio is 31. This is comparable to the best collimated jets from young stars (e.g. Reipurth 1991). It is remarkable that outflow phenomenae of such similarity occur both at the beginning and the end of a star's life, and it is of interest to compare the jets of M 2-9 in more detail with those from young stars.

There are four principal similarities: Firstly, the high degree of collimation. It is still not fully understood how the copious mass loss from young stars gets collimated into jets, but most models require the presence of a magnetic field. It is not known if magnetic fields are present around the source of M 2-9. If the source is a binary, additional mechanisms for collimation may be possible. Secondly, the ejection velocity and dynamical age of the ansae of M 2-9 are very similar to those known for Herbig-Haro objects from young stars. Third, the ansae show evidence for a slight, gradual change in the direction of illumination, because the NW side and the SE side are both brighter. This suggests that the central source (or the flow channel in the circumstellar material through which ejecta and light escape) may be precessing, a phenomenon that is often suspected in young outflows, and is a natural property of binaries. Finally, young stars have also been observed to contain light scattered from dust in their outflows. For instance, in HH1/2 Solf & Boehm (1991) observed scattered light within emission lines, which was subsequently modeled by Noriega-Crespo et al. (1991)

On the other hand, significant differences also exist. In M 2-9 we do not see a chain of bow shocks, only one in each extended lobe. Multiple bow shocks are often seen in flows from young stars (and in at least one case also from evolved stars, namely that of M1-16 (Schwarz 1992)), and are probably caused by a series of consecutive accretion events in the underlying source (e.g. Reipurth 1989). The mass loss history of evolved stars is likely to commence with a slow, poorly collimated wind, which later may be penetrated and overtaken by fast, and better collimated mass ejecta.

The main difference between the flow in M 2-9 and those from young stars, however, is that the M 2-9 flow is not shocked, but is seen only by reflected light. This is remarkable and not easily understood, If a wind moves with a velocity of 164 kms^{-1} into a stationary medium a shock will inevitably result. If the ambient medium is co-moving, the shock velocity will equal the difference in velocity of the wind and the medium. Therefore, only if the ambient medium is moving with almost the same velocity as the ansae would the shock be so weak as to emit negligibly, except possibly in infrared H_2 emission. However, our unpublished K images of the M 2-9 ansae show them to be extremely faint, precluding the presence of any strong H_2 line emission. But the current fast wind was most probably preceded by a much slower wind, and their interaction would certainly cause shocks to form. A more probable scenario is therefore that the bipolar jets in M 2-9 actually were shocked flows in the past until they burst through the region of the slow wind. Presently the ansae are thus travelling beyond the reach of the slow wind, and through the interstellar medium, which must be so tenuous that the shock is unobservable. This is partly because the ansae interact with so little ambient material, and partly because the physical extent of the shock is too small to produce much emission along the line of sight. Dust can be destroyed within powerful shocks, so it is possible that the dust presently visible in the two extended outflow lobes could have formed within the last few hundred years or however long it has been since the fast lobes overtook the slow wind material. Entrainment of the dust is an other possibility for it to survive for a significant time. In any case, it is conceivable that dust formation is facilitated by the large amount of processed material ejected from the central source, again a major difference with respect to the flows from newborn stars.

Acknowledgements. Our thanks go to R.Barbon for donating some observing time at the ESO 3.6m telescope to obtain the polarization measurements.

References

Acker, A. et al. 1992 ESO-Strasbourg Catalogue of Galactic PNe.
Allen, D.A. & Swings, J.-P. 1972 ApJ 174,583
Aspin, C., McLean, I.S. 1984 AA 134, 333
Balick, B. 1989 AJ 94, 671
Barker, T. 1978 ApJ 220, 19
Bergh, S. van den 1974 AA 32, 351
Calvet, N. & Cohen, M. 1978 MNRAS 182, 687
Carsenti, U., Solf. J. 1983 IAU Symp. 103, 510
Ciatti, F. & Mammano, A. 1975 AA 38,435
Di Bartolomeo, A., Barbaro, R., Perinotto, M.: 1996, MNRAS, in the press
Code, A.D. & Whitney, B.A. 1995 ApJ 441,400
Goodrich, R.W. 1991 ApJ 366, 163
Henyey, L.G., Greenstein, J.L.: 1941, ApJ 93, 70
Kohoutek, L. & Surdej, J. 1980 AA 85, 161
Lutz, J.H., Kaler, J.M., Shaw, R.A., Schwarz, H.E., Aspin, A. 1989 PASP 101, 966
Minkowski, R. 1947 PASP 59, 257
Noriega-Crespo, A., Boehm, K.-H., Calvet, N. 1991 ApJ 379, 676
Reipurth, B.: 1989, Nature 340, 42
Reipurth, B.: 1991, in *The Physics of Star Formation and Early Stellar Evolution*, eds. C.J.Lada & N.D.Kylafis (Kluwer, Dordrecht), p.497
Schwarz, H.E. 1984 PhD thesis, University of Glasgow.
Schwarz. H.E. 1990 in From Miras to PNe. p.536 Ed. M.O.Mennessier
Schwarz, H.E. 1992 AA 264, L1
Schwarz, H.E. 1994 34th Herstmonceux Conf.Proc. Eds. R.E.S. Clegg et al.
Schwarz, H.E., Corradi, R.L.M., Stanghellini, L. 1993 IAU Symp. 155, 214
Solf, J. 1993 Capri meeting on Outflows.
Solf, J., Boehm, K.-H. 1991 ApJ 375, 618
Swings, J.-P., Andrillat, Y, 1979 AA 74, 85
Trammell, S.R., Goodrich, R.W., Dinerstein, H.L. 1995 ApJ 453, 761
Walsh, J.R. 1981 MNRAS 194, 903

This article was processed by the author using Springer-Verlag LaTeX A&A style file *L-AA* version 3.